UAS SURVEYS REVEAL HIGH SPATIOTEMPORAL VARIABILITY IN BEACH MORPHOLOGY INCLUDING SUBCELL SAND EXCHANGE AND ACCRETION DURING SWELL EVENTS: WAIKĪKĪ, HAWAIʻI

A THESIS SUBMITTED TO THE GRADUATE DIVISION OF THE
UNIVERSITY OF HAWAIʻI AT MĀNOA IN PARTIAL FULFILLMENT
OF THE REQUIREMENTS FOR THE DEGREE OF

MASTER OF SCIENCE

IN

GEOLOGY & GEOPHYSICS

AUGUST 2020

By

Kristian Kainalu McDonald

Thesis Committee:
Charles Fletcher, Chairperson
Tiffany Anderson
Scott Rowland

Keywords: UAS, UAV, beach surveys, coastal monitoring, coastal management, structure from motion, Waikīkī, Hawaiʻi

ACKNOWLEDGEMENTS

Thank you to the Hauʻoli Mau Loa Foundation for giving local, underrepresented students a chance to pursue higher education. I could never have dreamed of the opportunities I've had throughout my graduate studies. I would absolutely not be where I am today if it weren't for the assistance the Foundation provided.

I'd like to thank my advisor Dr. Chip Fletcher. You took a chance on me way back in my junior year of my undergraduate studies and it's been filled with amazing experiences ever since. Throughout this project, your patience, positivity, and dedication to your work encouraged me to go on when I felt I no longer could. Thank you for believing in me and my ability, even when I didn't.

I'd like to thank Dr. Tiffany Anderson. Tiff, this project would not have been possible without your support. You never thought twice to go out of your way to help me or answer any questions I had. You are an incredibly humble and talented scientist and mentor and continue to be an inspiration to me.

I'd like to thank Scott Rowland. Your passion for science and ensuring the success of your students is nothing short of inspiring. You are very much an asset to this department and you have been a wonderful committee member.

I'd like to thank Korey Wong for not only being a great friend, but also for getting up excruciatingly early to survey every week for 8 months.

I'd like to thank Matt Barbee for your mentorship in the earliest stages of my graduate studies. Your ideas inspired this work and you helped me believe that I was capable of pursuing it.

I'd like to thank Haunani Kane. You've taught me that one of the most important parts of science is to think outside the box. You've taught me to believe in yourself, who you are, and where you come from and to not be afraid to let it bleed into your work.

I'd like to thank my parents, Makani and Lori, and my sister Crystalle. You've taught me that success, more than anything else, is being happy with who you are and where you are in the moment. I love you guys.

I'd like to thank my partner Jessi Lizama. Through thick and through thin, your undying support has truly been special. Teamwork really does make the dream work!

I'd like to thank Arlene Sullivan. You've made so many of my experiences possible, from helping with purchasing equipment, sorting out airfare and fees for conferences, assisting with forms, the list goes on.

I'd like to thank all the friends I've made along the way through my academic journey here at the University of Hawaiʻi and beyond. You've provided amazing memories throughout this time that I will never forget.

There is an endless number of people to thank. I could never be where I am today without the loving support from my family, friends, and colleagues. To all of those who've inspired me in one way or another, this is dedicated to you.

ABSTRACT

More than 70 percent of Hawaiian beaches are chronically eroding due to both natural and anthropogenic causes. Small unmanned aerial systems (sUAS) provide an efficient way to reveal processes controlling the morphology of these sandy shorelines so that they can be more effectively managed. One of Hawai‘i’s most popular tourist destinations, Waikīkī’s Royal Hawaiian Beach, suffers from chronic erosion and requires regular nourishment to prevent complete beach loss. To evaluate the efficacy of using consumer-grade sUAS to monitor subaerial sand volume and processes that drive beach morphodynamics, we conducted weekly aerial and ground surveys from April to November 2018 from which high-resolution point clouds, digital elevation models, and orthomosaics were generated. Our observation period brackets the season of high swell thought to largely control annual beach behavior in Waikīkī. Using empirical orthogonal function (EOF) and surface variability analyses, we describe subcell behavior within the greater littoral system that has not previously been observed. Despite being characterized as a chronically eroding beach, net gains of surface area and sand volume were observed over the course of the 8-month monitoring period (708.5 ± 43.5 m^2 and 1384.8 ± 102.2 m^3, respectively). These gains were due to seasonal swell activity and a relatively active hurricane season. We also quantified and compared shorter-duration volume gains and losses due to swell events, hurricanes, and wind variability. Considering its economic value and the expected exacerbation of erosion as sea level rises, information provided through sUAS surveys will likely become integral to coastal zone managers as they develop strategies to preserve Waikīkī’s Royal Hawaiian Beach.

Plain-language summary:

As beaches erode due to both natural and human causes, unmanned aerial systems (UAS), also known as drones, will be an integral tool in helping coastal communities develop effective management strategies. One of Hawai‘i’s most popular tourist destinations, the Royal Hawaiian Beach in Waikīkī, is experiencing chronic erosion. To better understand this problem, we collected weekly observations using survey equipment coupled with photos taken by UAS and analyzed how the beach changed from April 2018 to November 2018. We found that the eastern

and western halves of the beach behave somewhat independently of each other, but may share sand in subtle ways. The size of the beach was smallest at the beginning of the monitoring period prior to any influence of seasonal swell and increased in both volume and surface area as waves associated with southern hemisphere storms, hurricanes, and winds, added sand to the beach, thus greatly altering its capacity as a recreational and ecological asset. This study shows that UAS are a cost-effective and efficient management tool for the coastal zone.

TABLE OF CONTENTS

LIST OF FIGURES

1. INTRODUCTION

Beaches are highly dynamic systems, constantly changing in response to marine forces. As many of the world's beaches are the site of urban and suburban areas located just meters from the water's edge, it is necessary to improve understanding of beach behavior on a range of temporal and spatial scales. Waikīkī, located on the south shore of O'ahu, functions as the premier resort destination of the Hawaiian Islands, generating an estimated $2.2 billion in visitor expenditure per year (Tarui et al., 2018), while also serving as a cultural and recreational hub for both visitors and residents alike.

Some 70 percent of beaches in Hawai'i are chronically eroding due to both natural and anthropogenic causes (Fletcher et al., 2012). Year-to-year erosion in Waikīkī has required regular intervention to retain sediment and beach function for more than a century (Wiegel, 2008), and as a result, the area has been the subject of multiple scientific studies (Wang and Gerritsen, 1995; Miller and Fletcher, 2003; Habel et al., 2016). To date, however, traditional surveying methods have limited the spatial and temporal resolution of research and thus hampered understanding of more detailed beach processes. With the advent of consumer-grade small Unmanned Aerial Systems (sUAS) coupled with modern Structure-from-Motion (SfM) photogrammetry software, there is potential to understand beach behavior at a higher level of complexity and detail.

Coastal research using remote sensing and UAS platforms has been a rapidly evolving area of study. Early use of remote sensing techniques relied on time series of aerial and/or satellite imagery to determine temporal patterns of shoreline change and remains a useful method (Dolan et al., 1978, Coyne et al., 1999; Rooney & Fletcher, 2000; Genz et al., 2007; Romine & Fletcher, 2013). The development of Light Detection and Ranging (LiDAR) techniques allowed for the study of 3-dimensional subaerial and nearshore coastal variability (Stockdon et al., 2002; White and Wang, 2003), however, but are often cost prohibitive. High-frequency sampling intervals can be achieved with coastal monitoring stations, like the ARGUS system (Holman and Stanley, 2007), but require infrastructure and installation and can be subject to high vertical uncertainty (Harley et at., 2011).

Beginning in the mid-2000s, UAS, given their operational flexibility and versatility, began to be used to study coastal environments (Lomax et al., 2005; Delacourt et al., 2009).

Lower costs, associated with the growing demand for consumer-grade sUAS, and improved accuracy relative to traditional survey methods (Beretta et al., 2018) have made these platforms more useful for studying coastal morphodynamics (Mancini et al., 2013; Casella et al. 2016). However, despite the capacity to collect data at higher (e.g. weekly, daily, etc.) temporal resolutions, there are few published studies of beach dynamics using sUAS at these frequencies.

Typical coastal monitoring methods have focused on broad scale beach response and morphological change (Dail et al., 2000; White and Wang, 2003; Turner et al. 2016). Here, we develop a modified methodology using sUAS that reduces field time compared to traditional methods, allowing for rapid data collection. The method produces accurate 3-dimensional reconstructions of the subaerial beach with high spatial resolution. The objectives of this study are (1) develop a rapid, low-cost coastal monitoring methodology using sUAS, (2) identify patterns of morphological variability with weekly temporal resolution, (3) correlate quantitive measurements of subaerial beach variability with marine forcing and (4) advance understanding of morphodynamics on reef-fronted beaches.

2. SITE DESCRIPTION

Royal Hawaiian Beach is a crescent-shaped, carbonate sand beach located in the heart of Waikīkī (Figure 1). Bound by two groins, it is a compartmentalized littoral cell extending 520 meters, with terminal structures preventing significant longshore transport into or out of the system (Habel et al., 2016). Any net sediment gain or loss occurs primarily through cross-shore transport (Environmental Assessment, 2010); however, pronounced longshore sediment exchange within the cell does create localized erosion and accretion hotspots depending on short-term fluctuations in the wave field (Habel et al., 2016).

Typical sand in the study area is characterized as moderately-well to well sorted medium sand (D_{50}: 0.29 - 0.40 mm), with notably coarser grains near the terminal groins (D_{50}: 0.80 mm; Environmental Assessment, 2010). Royal Hawaiian Beach has a long history of sand nourishment. Most recently in 2012, the State of Hawai‘i brought 17,551 m^3 of carbonate sand from a reef-top borrow site located approximately 200 m offshore (Habel et al., 2016). Some

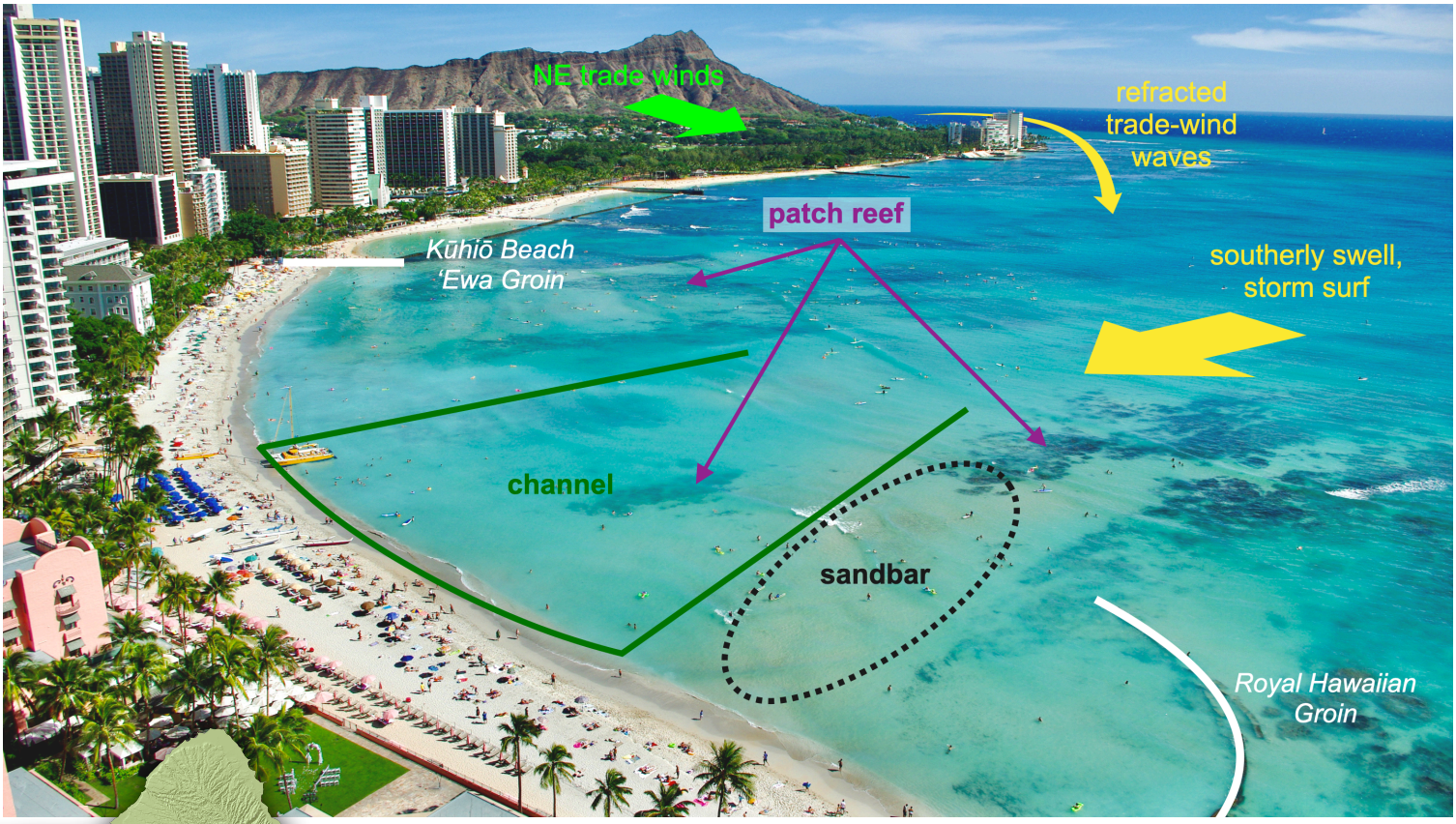

Figure 1. Looking Southeast above the Royal Hawaiian Beach. A crescent-shaped, carbonate sand beach located in the heart of Waikīkī on the south shore of O'ahu. It is a compartmentalized littoral cell, with terminal structures (Kūhiō Groin and Royal Hawaiian Groin) preventing significant longshore transport into or out of the cell. The nearshore is complex, with patch reefs, a shallow submarine channel, and a perennial sandbar adjacent to it. These features interact with wind-generated waves produced by persistent northeasterly trade winds in addition to southerly swell during the summer months and storm surf, typically during hurricane season (June - November).

compaction and grain breakage was observed resulting from the transport of sediment during the recent nourishment.

The nearshore is characterized by a wide and relatively shallow (1-3 m in depth) carbonate reef platform, an irregular patchwork of fossil reef outcrops separated by mobile and largely thin (<1 m-thick) sand deposits, extending more than 1000 meters offshore. The platform is bisected by a shallow submarine sand field sitting in the former location of a freshwater stream that flowed through the area when sea level was lower ('Āpuakēhau Stream; Clark, 1977). This sand field is thought to be a conduit for cross-shore transport, contributing to an average

shoreline recession (erosion) rate of 0.7 m/yr and annual sediment loss of about 1070 m^3 (Environmental Assessment, 2010).

The complex bathymetry produces complicated wave and current conditions. Previous studies have shown that a wave-induced longshore current typically flows to the northwest at velocities generally below 0.15 m/s (Gerritsen, 1978), but this current will reverse on occasion due to seasonal changes in swell direction (Gerritsen, 1978; Miller and Fletcher, 2003).

The dominant swell regimes for the Hawaiian Islands are depicted in Figure 2. Southerly swells generated by storms in the southern hemisphere represent the greatest source of wave energy to the study site. These waves are most prevalent between April and October, occurring 53 percent of the time during a typical year (Homer, 1964). Often traveling more than 8000 kilometers, they have deep-water wave heights ranging from 0.3 to 1.2 meters, with periods of 14 to 20 seconds (Environmental Assessment, 2010). Wave direction depends on storm position and track, with resulting swells typically approaching from between the southeast to southwest.

Locally-generated wave resulting from trade-winds blowing from the east or northeast occur 75% of the time during a typical year (Homer, 1964) and are most persistent through summer months (Environmental Assessment, 2010). Deep-water wave heights associated with trade-wind waves are typically 0.9 to 2.4 meters with periods of 5 to 10 seconds. The study area, in the lee of the island, is mostly sheltered from this energy, although some trade-wind wave energy is refracted around the southeastern end of the island (Environmental Assessment, 2010).

Occasionally, storm-generated waves can affect the Waikīkī area via Kona storms or tropical cyclones. Kona storms typically occur during the winter season when low pressure systems travel across the North Pacific Ocean and track to the south of the Hawaiian Islands. These storms occur 10 percent of the time during a typical year (Homer, 1964) and are associated with strong southerly and southwesterly winds capable of generating deep-water wave heights of 1 meter with larger waves ranging from 3 to 5 meters and periods of 8 to 10 seconds (Gerritsen, 1978).

Hurricanes, usually spawned in the eastern or central tropical Pacific Ocean, occur during the months of June to November. Hurricanes that travel west into the Central North Pacific Basin have historically passed south of the islands and are capable of producing large surf in the study

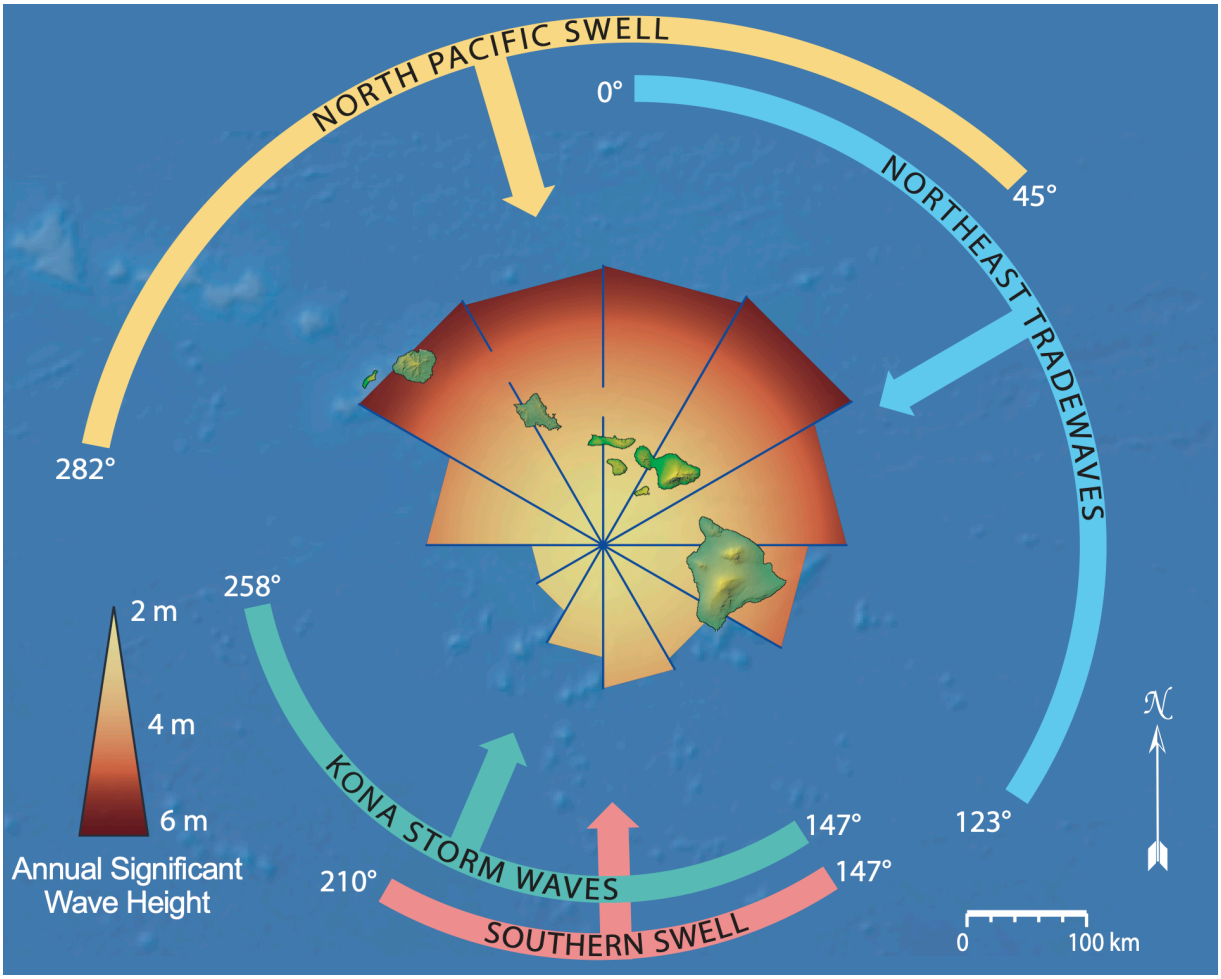

Figure 2. Dominate swell regimes for the Hawaiian Islands. Southerly swell generated by storms in the southern hemisphere represent the greatest source of wave energy to the Royal Hawaiian Beach. Occasionally, storm-generated waves can affect the Waikīkī area via Kona storms or tropical cyclones. Refracted wave energy due to locally-generated northeasterly wind-driven waves are also capable of influencing the study site. Northerly swells, typical during the winter season, are mostly blocked by the island and have little influence on the beaches of Waikīkī; however, swells with an extreme westerly or easterly direction may generate some refracted energy into the cell. After Vitousek & Fletcher (2008), based on Moberly & Chamberlain (1964).

area. Modeling suggests they are (or will be) migrating north toward the latitude of the Hawaiian Islands due to climate change (Murakami et al., 2013).

The 2018 hurricane season, with 23 named storms, was the fourth most active season on record and produced the highest accumulated cyclone energy value on record in the Central Pacific basin (NOAA, 2019). Three storms impacted the study site during our monitoring period. Hurricane Hector reached Category 4 intensity and passed south of O‘ahu in mid-August, generating deep-water waves that peaked at 1.25 meters in height from a south-southwesterly direction (200º-213º). Hurricane Lane occurred at the end of August and attained Category 5 intensity, sending the largest swell of the study period with deep-water heights of just over 2

meters from the south-southwest (190º-210º). The third storm to influence the study site was Hurricane Walaka, passing to the south in September and early October. This storm also attained Category 5 intensity and sent the second largest swell of the observation period, with peak deep-water heights just under 2 meters from a southwesterly direction (210º-227º).

Northerly swells, generated by winter storms in the northern hemisphere, produce deep-water waves heights as great as 9 meters at periods of 12 to 20 seconds (Environmental Assessment, 2010), but are mostly blocked by the island and have little influence on the beaches of Waikīkī. Swells with an extreme angle of approach, however, may generate some refracted energy into the area.

The beach generally experiences erosion under shorter period wind-driven winter waves arriving from the northeast, and recovery in the summer during the time of longer period southerly swell (Habel et al., 2016; Miller and Fletcher, 2003; Norcross et al., 2003). In a study of the 2012 nourishment, Habel et al. (2016) found that seasonal changes in the wave field caused the beach volume to fluctuate by 2000 - 4000 m^3 (15 percent to 30 percent of total nourishment addition) over the course of 2.7 years. Total beach volume decreased at a rate of 760 ± 450 m^3/yr. Additionally, they observed a long-term east-to-west transport accompanied by cross-shore transport, with nearshore sand fields acting as both a sand source (during storm-related swell events) and sink (during non-storm periods) depending on seasonal conditions.

3. METHODOLOGY

3.1 SURVEYING

We ran a weekly monitoring program from mid-April to the end of November of 2018 using consumer-grade sUAS, capturing the effects of both seasonal and hurricane-generated waves. The initial survey was conducted about one week prior to the first significant southerly swell of the summer season to establish a baseline beach state, with 26 subsequent weekly surveys thereafter.

Aerial surveys were conducted using a Phantom 4 Pro, a consumer-grade quad-rotor sUAS manufactured by Dà-Jiāng Innovations, commonly known as DJI. This sUAS was chosen due to its availability and ease-of-use, relatively long flight time (~30 minutes), stock 3-axis

gimbal with a 20-megapixel red-green-blue (RGB) sensor, and compatibility with 3rd-party flight planning software. Additionally, the sensor utilizes a global shutter, meaning that all pixels of the image sensor array are exposed simultaneously, enabling the capture of moving targets without the spatial distortion that can be experienced from rolling shutters of previous Phantom model sensors. This results in improved accuracy and reduced image processing times (Vautherin et al., 2016).

Flights were semi-automated using the flight planning software package DroneDeploy with shore normal tracks, collecting still imagery with 80 percent overlap in both x and y. Flight height was set at 120 m above ground level, allowing clearance of buildings and other structures while optimizing image resolution and maintaining FAA airspace compliance. Camera parameters were dependent on conditions and lighting, but high shutter speeds (1/1000 - 1/600) were used to reduce motion blur of objects and distortion introduced by the movement of the image collection system.

Seven 1 x 1 meter vinyl targets were placed at equidistant intervals along the length of the subaerial beach and functioned as ground control for each aerial survey. The seaward boundary of the subaerial beach was defined as the low water mark (LWM), or the toe of the beach, which is typically used as a proxy for shoreline change analysis along Hawaiian coastlines (Fletcher et al., 2012). The LWM measurements, collected every 2-3 m, and ground control points were surveyed in the field using a rod-mounted prism and a Leica TS16 Robotic Total Station. Survey timing was random with respect to wave state and tidal cycle. Existing benchmarks were used to orient the spatial reference using the WGS 1984 UTM Zone 4 projection. Elevations were measured with respect to local mean sea level (LMSL; Datums - NOAA Tides and Currents, n.d.).

3.2 3-Dimensional beach reconstruction

Point clouds and orthomosaics were produced using Photoscan (now Metashape), a photogrammetric processing application developed by Agisoft LLC. The process generally follows a methodology developed by the United States Geological Society (USGS, 2017a; USGS, 2017b), in which imagery taken by sUAS is combined with surveyed control points in an

iterative process to reduce errors and produce map-quality 3-dimensional surface reconstructions. Dense point clouds were then exported for additional processing using Rapidlasso's LAStools, a software suite allowing for batch-scriptable, multi-core processing of point cloud data. The automated LAStools processing involved standard remotely sensed data processing (e.g. masking, thinning, and classifying) of the point cloud in addition to the removal of noise introduced at the foreshore due to saturated sand and wave run-up. Manual assessment and removal of any residual noise was conducted for each post-processed point cloud.

Post-processed point clouds were imported into ESRI's ArcMap and merged with the surveyed LWM points. Digital elevation models (DEMs) with 0.5 meter cell sizes were generated using natural neighbor interpolation and smoothed using mean cell values located within a 5 m radius circular neighborhood so as to reduce noise and to reveal larger-scale patterns of variability. The DEM time series was used for all analyses including width, volume, surface area, surface variability, and empirical orthogonal function (EOF) analysis.

3.3 Beach width, volume, and surface area calculations

Beach width, volume, and surface area were calculated for the subaerial (dry) beach above the mean higher high water (MHHW) tidal elevation. MHHW, which is measured at 0.329 m above LMSL at the nearby Honolulu tide gauge (NOAA Tides and Currents, 2003), is used to represent an upper bound of present-day sea level in coastal studies of the urban corridor of O'ahu (PacIOOS, 2016). Beach width, calculated at 5 meter intervals along the beach, was the distance between the seaward edge of the beach (where the beach surface intersects the MHHW elevation) and the inland edge of the beach (typically identified by cement walkways or other engineered structures). Volume and surface area were calculated relative to MHHW using the ArcGIS tool "Surface Volume".

3.4 Uncertainty

To quantify error in the sUAS-derived DEMs, a separate survey was conducted, in which elevation measurements were taken randomly throughout the study area using a Leica TS16 Robotic Total Station, which results in millimeter-level accuracy. Simultaneously, sUAS imagery

and ground control points were collected, from which a DEM was created following the method presented in this study.

Errors in DEM elevations were calculated by taking the measured total station elevations, assumed as real, and subtracting from them the DEM elevations at the same location. The mean of the errors was effectively zero (0.007 m), and measured locations were sufficiently spaced that there were no observed spatial correlations between adjacent error values. Thus, the measured errors can be considered to be randomly distributed about a mean of zero.

From these randomly distributed errors, the uncertainty in beach width is quantified by determining the upper and lower bounds of beach width. The smaller bound is the width of the beach whose seaward edge intersects the MHHW + σ_μ elevation contour; the width of the beach whose seaward edge intersects the MHHW - σ_μ constitutes the larger bound. Beach width uncertainty is then one-half the difference between the width of the upper and lower bounds.

Similarly, The uncertainty in the surface area was determined by recalculating surface area for each DEM using seaward boundaries of MHHW + σ_μ and MHHW - σ_μ. Uncertainty was calculated as one-half the difference between these two values.

The uncertainty in sediment volume from each DEM is estimated as

$$U_{vol_j} = A_j \sigma_\mu \qquad (1)$$

where A_j is the footprint, or area, of the j^{th} sUAV-derived DEM of the subaerial beach, and σ_μ is the standard deviation of the mean of errors, $\sigma_\mu = \sigma/\sqrt{n}$, where σ is the standard deviation of the errors themselves, and n is the number of total station elevation measurements.

3.5 Empirical orthogonal function analysis

We use empirical orthogonal function (EOF) analysis to quantify spatiotemporal modes of variability of the subaerial beach. EOF analysis is a common method for analyzing the variability of a single value (i.e. elevation) and is often used to study beach profile evolution (Winant et al., 1975; Aubrey, 1979; Dick and Dalrymple, 1984; Losada et al., 1991; Norcross et al., 2003; Anderson et al., 2009). As is standard in EOF analysis, the time average was removed

in order to describe variations from the mean beach. Our analysis focuses on the first four modes of variability which represent 82 percent of the total data variance.

3.6 Shoreline response to wave forcing

Beach volume and surface area calculations, DEM surfaces, and EOF modes of variability were compared to regional wave and wind conditions to determine morphological response of the beach. Regional hourly modeled significant wave height, mean direction, and mean period were obtained from the Pacific Integrated Ocean Observing System (PacIOOS) program at the University of Hawai‘i at Mānoa (Wave Forecast). Atmospheric parameters from the National Centers for Environmental Prediction (NCEP) Global Forecast System weather model are used to force higher resolution WaveWatchIII and Simulating Waves Nearshore (SWAN) wave models for the island of O‘ahu. The high-resolution (500 m) SWAN model was developed to capture shallow water effects and nearshore coastal dynamics such as refracting, shoaling, and smaller scale shadowing (SWAN Regional Wave Model, 2010). Regional hourly wind speed and direction were obtained from the Weather Research and Forecasting (WRF) model, a 1.5-km resolution open source numerical weather prediction system, also via PacIOOS (Wind Forecast). The data were obtained for the grid cell most proximate to the study area (21.27º N, 157.827º W) following Habel et al. (2016).

4. RESULTS

4.1 Variation in beach width

The beach width for each transect in each survey (Figure 3) was subtracted from each transect’s mean beach width of the time-series. These differences from the mean are shown in Figure 4. Each grid cell represents one transect (x-axis) on a particular survey date (y-axis), while the colors correspond to widths narrower than the mean (red) and widths wider than the mean (blue).

Each transect’s width fluctuated throughout the study period, varying from their respective means by as many as 3.5 meters. Most transects from surveys early in the time series (April-June) were narrower than their means, particularly at the west end (transects 1 to 30) and

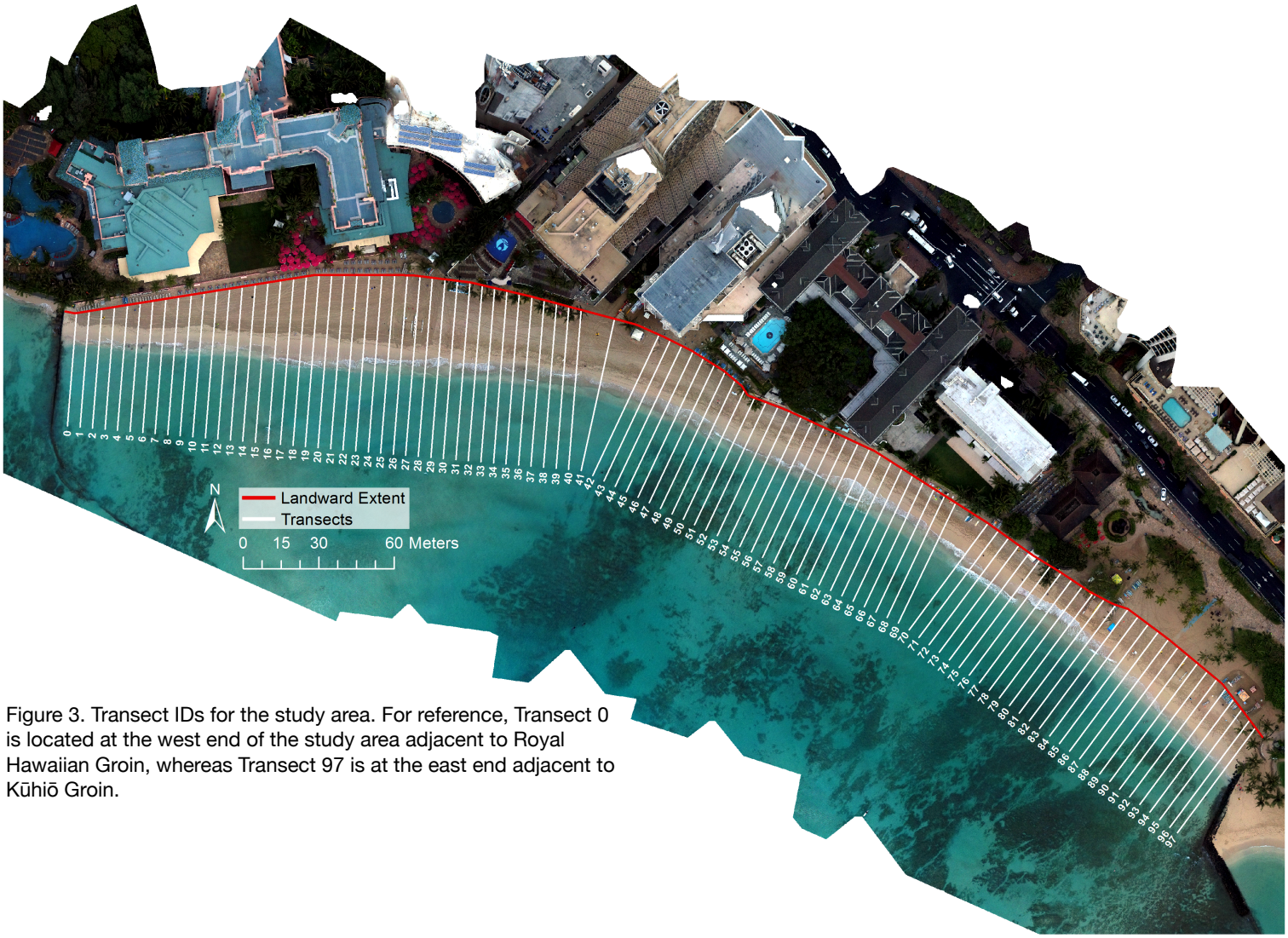

Figure 3. Transect IDs for the study area. For reference, Transect 0 is located at the west end of the study area adjacent to Royal Hawaiian Groin, whereas Transect 97 is at the east end adjacent to Kūhiō Groin.

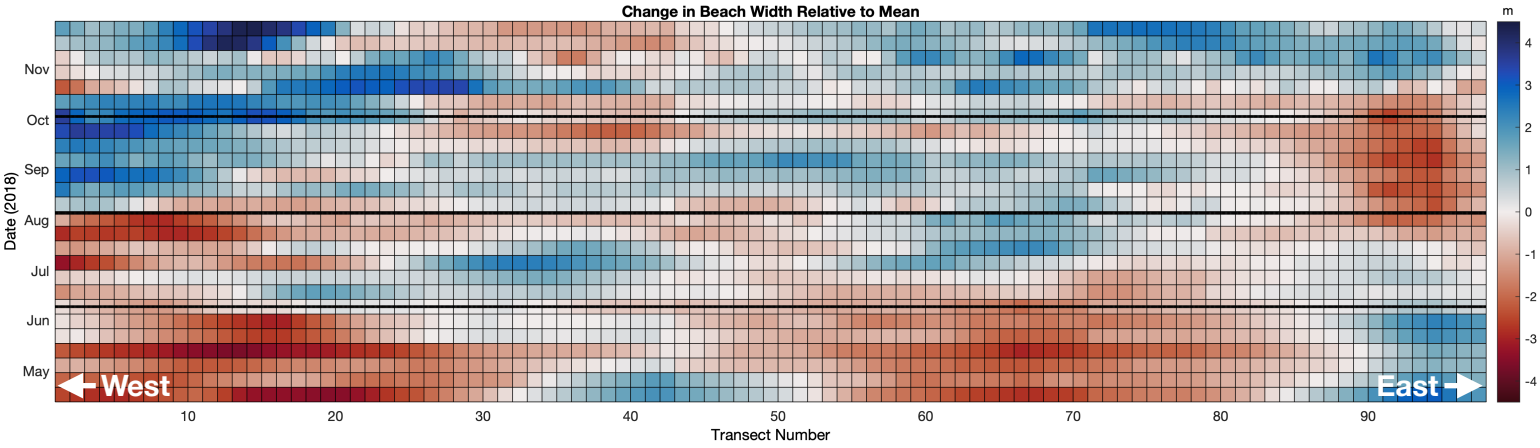

Figure 4. Differences from mean beach width for each transect across the DEM time series. MHHW was used to represent the seaward extent of the beach. The first survey is represented by the bottom row and subsequent surveys are represented by each row above thereafter. For spatial reference with Figure 1, Transect 0 is represented by the left-most column.

just east of the central region (transects 55 to 85). Between these narrower regions was an area (transects 35 to 45) in which transects were slightly wider than their means for 2 weeks. The transects on east end of the study area (transects 90 to 97) were also wider relative to their means, persisting until the beginning of July.

Later in the summer (late-June to early July), these narrower and wider regions began to dissipate. Then, in mid-July, just before the midpoint of the survey period, the beach began to narrow at east end (transects 85 to 97) and maintained this narrowed state until mid-October after which it recovered and began to widen before end of the study period in November. The narrowed state at the west end slowed briefly in late-June before intensifying in early July through the beginning of August. Somewhat abruptly, this region began to widen, and maintained this widened state until the end of the survey period. Overall, the second half of the survey period was characterized by a gradual shift in beach width from a pattern narrower than the mean to one that was wider than the mean for the majority of the study area.

4.2 Variation in elevation

To identify temporal patterns of elevation change, the spatial variation in elevation about the mean was determined for four quarters, each spanning roughly 8 weeks. Figure 5 shows the differences between the quarterly mean elevation for each pixel and the mean elevation during the entire time series for each pixel. Red and blue correspond to decreases and increases in elevation, respectively.

Generally, the data show that changes in elevation were restricted to the portion of the beach that was influenced by the wash of the waves. Wave run-up was capable of traveling as much as 20 meters above the MHHW line, depending on beach slope, tide, and wave conditions. Quarter 1 (Figure 5a) was characterized overall by elevations that were lower than the mean, with the exception of two small regions at the east end of the beach and immediately west of the center of the beach that were higher than the mean.

The pattern in the west half of the beach remained relatively unchanged from Quarter 1 to Quarter 2, although the high and low contrast both decreased (Figures 5a and 5b). In the east

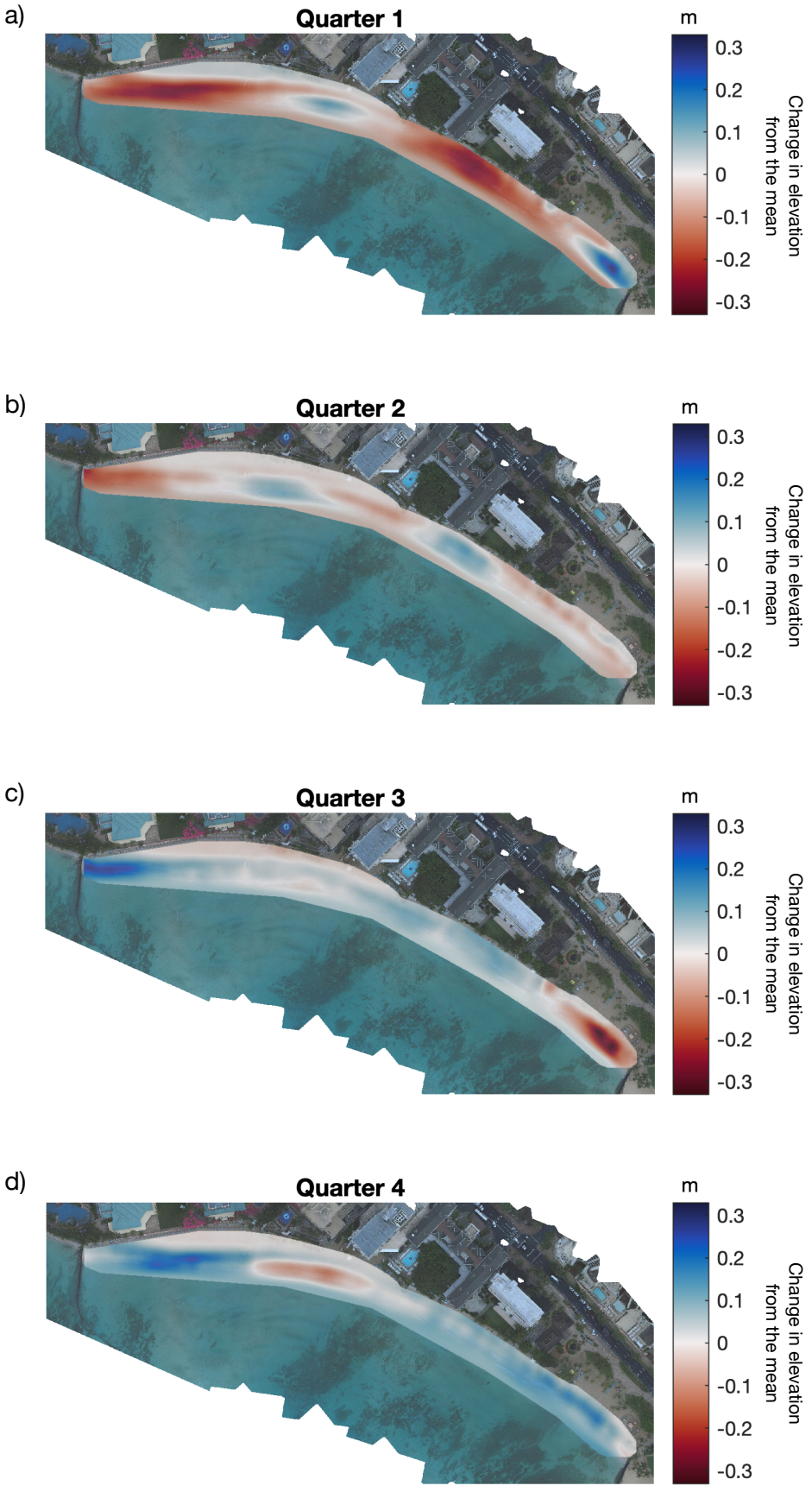

Figure 5. Quarterly elevation differences from the mean DEM. Red and blue represent elevations below and above the mean elevation of the quarter, respectively.

half, however, elevation patterns reversed from Quarter 1 to 2: the east end showed slightly lower elevations, while the west end showed slightly higher elevations.

Quarter 3 (Figure 5c) was characterized by an overall increase in elevation across most of the beach, especially at the far west end of the beach. However, the far east end of the beach continued to lower.

The beach during Quarter 4 (Figure 5d) remained relatively unchanged, with the exception of a slight decrease in elevation immediately west of the central portion of the beach and a building of the east half to elevations slightly above the mean along its entire length.

In comparing the general spatial patterns across each quarter, it appears that the beach varied in elevation in predominantly four distinct locations: two regions on the east half of the beach, and two regions on the west half of the beach. At the very center of the beach, there was an area of relatively little change that is consistent across the quarters, an apparent border between areas of larger variations in elevation, which appears to correspond with a nearshore patch reef that abuts the subaerial beach.

4.3 Changes in surface area and volume

To get additional perspective on forcing related to wave and wind characteristics, we examined changes in subaerial beach area and volume over the monitoring period relative to the initial survey (Figure 6). Overall, there was a gradual increase in area and volume throughout the time series: the beach gained 708.5 ± 43.5 m^2 (area) and 1384.8 ± 102.2 m^3 (volume). These trends were interrupted by short-lived erosion events, after which the gradual increases continued. The rate of recovery differed after each erosion event, but recovery within 2-3 weeks was typical. As the beach accreted and eroded, the surface area and volume trends were more or less parallel, particularly during the first half of the study period. During the second half of the study period, there were a few instances where trends crossed, mostly due to more rapid increases and decreases in surface area.

The relationship between forcing (wind and wave conditions) and beach response (changes in area and volume) is complex. Two examples illustrate this. 1) There are at least two occasions (April 26 to May 2; August 29 - September 21) where trade-wind variability (Fig. 6e

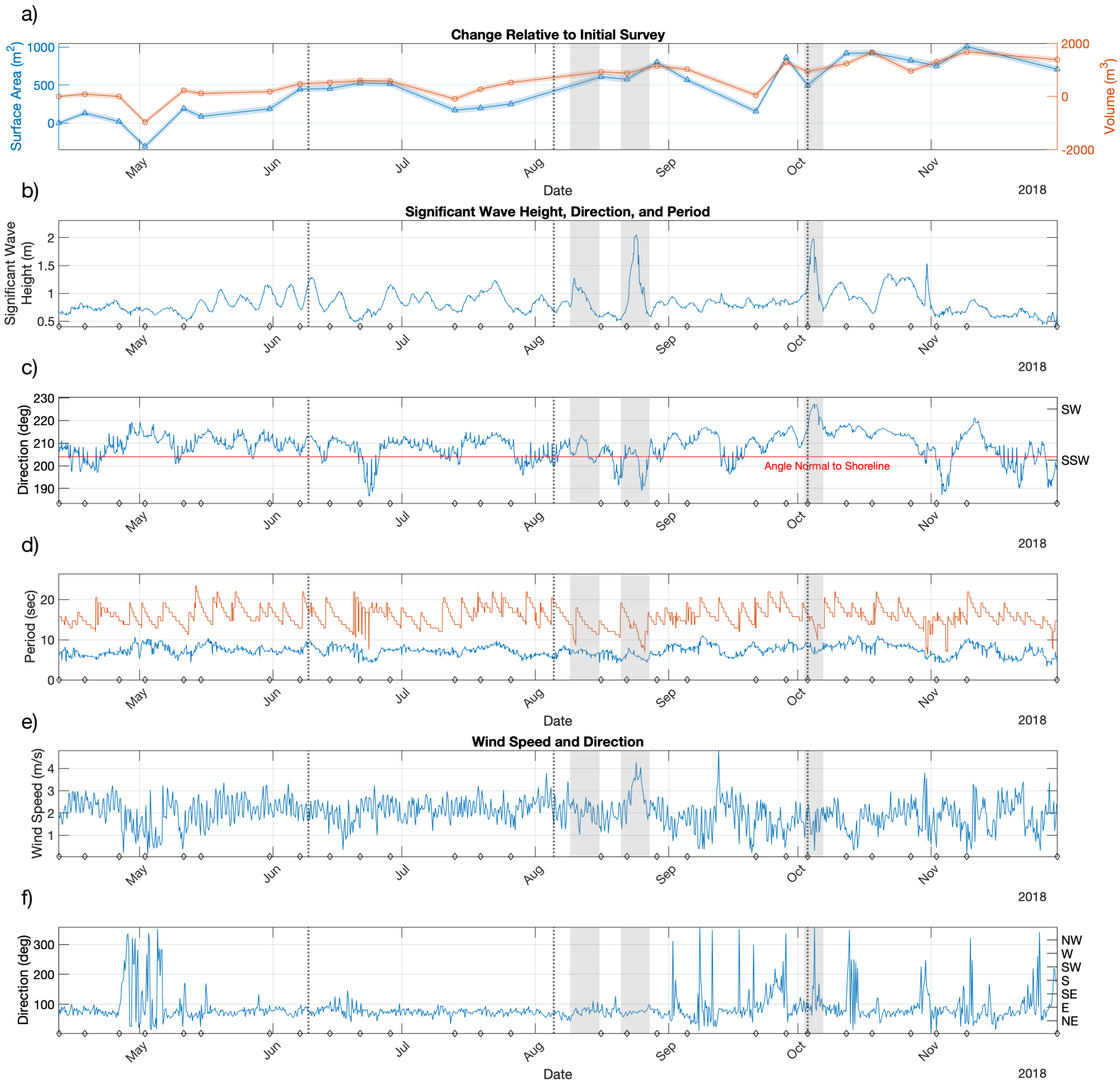

Figure 6. Surface area and volume plotted alongside the wave (height, direction, and period) and wind (direction and speed) conditions for the study period. Wave and wind data were obtained from PacIOOS for the nearest grid cell proximal to the study area following Habel et al. (2016). Hurricanes (Hector, Lane, and Walaka, respectively) are delineated in grey.

and f) coupled with weak southern hemisphere swell (Fig. 6c) lead to pronounced decreases in beach area and volume. The same effect, however, was achieved under consistent trade-winds, with relatively larger southern hemisphere swell (June 28 - July 13). On another occasion (September 21 - 28), variability in the trade-winds direction coupled with weak southern hemisphere swell lead to gains in beach area and volume. 2) With regard to locally-generated hurricane swell, week-to-week resolution of surveys prevents precise attribution to individual hurricane events. However, on at least three occasions (August 9 - 15; August 20 - 27; October 2 - 6), hurricane-generated swell did not interrupt previously existing accretion trends, nor produce decreases in beach area or volume. We hypothesize that large short-period swells deliver sand to the beach, a finding consistent with Habel et al. (2016), however additional research is needed to verify this behavior.

4.4 Empirical orthogonal function analysis

Figure 7 depicts the first four spatial modes and their respective temporal components derived from the EOF analysis, altogether representing 82 percent of the variability of the monitoring period. The maps in Figures 7a-d depict the spatial trends of each mode and are color-coded to indicate trends in erosion or accretion. For instance, in Figure 7a, the blue regions indicate a trend from erosion to accretion throughout the monitoring period and the red regions indicate a trend from accretion to erosion over the same period.

The first EOF spatial mode accounts for 51 percent of the total variance throughout the monitoring period. Figure 7a reveals vertical changes in the beach which we interpret as addition (accretion, blue) and removal (erosion, red) of sand. The pattern is in the form of two regions that share a boundary near the center of the beach. Each region has accreting and eroding portions. We interpret these as coherent sand-sharing “subcells” that appear to mimic each other in behavior. The juxtaposition of eroding and accreting portions suggest that within each subcell, eroding portions (red) are acting as sand sources to the accreting portions (blue). Within the two subcells, the overall pattern of this sand transport is from east to west.

With respect to the temporal pattern, we interpret the overall trend as one of accretion with sediment transport from the red areas, which are eroding, to the blue areas, which are

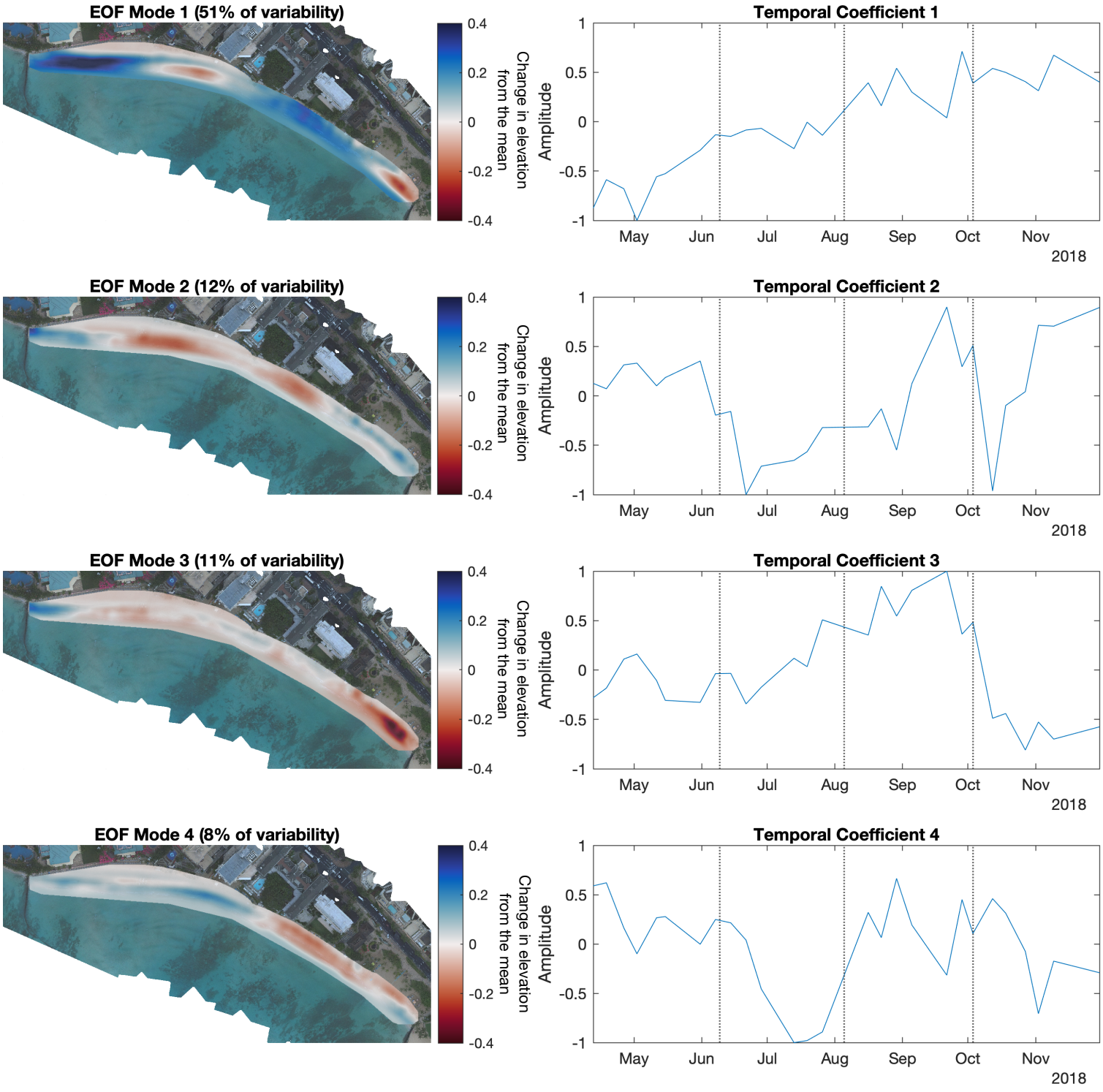

Figure 7. The first four spatial modes and their respective temporal coefficients of the EOF analysis, representing 82% of the variability of the study area during the course of the study period. For the spatial modes (left), the colors indicate trends seen over the course of the monitoring period. Red represent elevations below the mean, while blue represent elevations above the mean.

accreting. This trend of accretion is interrupted by occasional distinct short-term erosion events which typically recover within a matter of days to weeks. The last two months (October and November) show that the trend of accretion decreased and beach change became dominated by distinct short-term erosion events.

The second EOF spatial mode and its temporal coefficient reflect 12 percent of the total variability. Like the first spatial mode, two subcells are apparent. However, unlike the behavior of EOF mode 1, the sediment transport within the two subcells are mirror reflections of each other rather than replicating each other. Here again, the two subcells share a boundary near the center of the beach. In the mode 2 subcells, the ends of the beach accreted, apparently drawing sand from central regions of the beach and/or the nearshore.

Temporally, this spatial pattern persisted during the first two months of the monitoring period, with slight erosion near the center and steady accretion at the ends. This changed in the second week of June, when the central regions of the two subcells began to rapidly accrete while the east and west ends showed strong erosion. This pattern slowly dissipated until the beginning of September, and for the remainder of the monitoring period (late-September through November), the subcells took on characteristics similar to the first two months (erosion at the center and accretion at the ends). This late season trend was abruptly interrupted in October with a pronounced reversal that quickly ended as the trend was reestablished.

Representing 11 percent of the variability of the study area over the time series, the third spatial mode once more reflects two (relatively weak) subcells within the greater littoral system. These cells display opposing accretion and erosion at the ends of the beach, while the central area remained relatively unchanged. We interpret this as an indication that cross-shore sand exchange between the nearshore and subaerial beach is dominant, rather than the longshore transport that appears to have dominated in modes 1 and 2. This spatial pattern persisted until late July.

From July through September, subcell behavior reflected a trend of erosion on the east end of the beach, while the west end of the beach progressively accreted. This trend abruptly ended in late September, whereupon the beach returned to the spatial pattern seen from May through July for the rest of the monitoring period.

The spatial and temporal components of the fourth EOF mode represent 8 percent of the variability. This mode is characterized by two types of behavior: 1) A behavior of no net change (no trend) where there is little evidence of sand transport, neither along nor across the shoreline; 2) the appearance, once again, of two subcells sharing a common boundary in the central region, where the subcells reflect short-term trends of opposing erosion or accretion. That is, one subcell will be dominated by erosion while simultaneously the other subcell is dominated by accretion. Which subcell is dominated by which trend oscillates throughout the monitoring period. In our interpretation, behavior 1 is the more persistent (no trend), while behavior 2 is more event-based and of shorter duration. In behavior 2, it is unclear whether the two subcells are exchanging sand with each other or are in engaged in cross-shore sand exchange with nearshore sand fields. What is clear, however, is that the two subcells operate with opposite trends of erosion and accretion.

With respect to the temporal pattern, throughout most of the time series, there was oscillation of opposing accretion and erosion in the two subcells. The monitoring period began with the eastern subcell eroding and the western subcell accreting, but this quickly ended, and by the beginning of May the beach moved into behavior 1 (no trend). This persisted throughout May and June, but in early July, behavior 2 strongly developed, with the west subcell eroding and the east subcell accreting. By August, this pattern drew to a close, when it reversed back to the subcell pattern seen at the beginning of the monitoring period (accreting in the west and eroding in the east). This July event was pronounced in comparison to the other examples of behavior 2 throughout the monitoring period. From September through November, the subcells oscillated in behavior until the end of the monitoring period.

5. DISCUSSION

Previous studies of the Royal Hawaiian Beach (Gerritsen, 1978; Miller & Fletcher, 2003; Habel et al., 2016), using data with coarser spatial and temporal data resolution, came to the conclusion that the beach operated as a single, coherent littoral system dominated by a seasonal signal without additional complexity. The unique contribution of this study is that high resolution sampling and the construction of sub-meter resolution digital elevation models revealed the

presence of two subcells with a boundary in the central region, and that the subcells behave independently as revealed in EOF modes, particularly in modes 1, 2, and 4.

5.1 Subcell Detection

Prior to this study, variations in the morphology of Royal Hawaiian Beach were understood to consist of a seasonal response to changes in wave characteristics. During the winter season, the east end of the beach accretes and the west end erodes. This pattern reverses during the summer as southerly swells impact the shoreline (Miller and Fletcher, 2003; Habel et al., 2016). Habel et al. (2016) used EOF analysis to reveal underlying complexity, but spatial and temporal limitations in the quarterly dataset made it difficult to draw conclusions regarding higher resolution morphodynamics.

Our monitoring appears to be in agreement with the seasonal pattern observed in previous studies (i.e. accretion during the summer season). DEM analysis (Section 4.2) revealed that elevation variation appeared to be limited to four sections of the beach, with a distinct border at the central beach. In addition, use of empirical orthogonal functions to reveal subtle modes of beach behavior in our high resolution dataset uncover a complex sand exchange pattern consisting of two subcells operating within the greater littoral system. Whereas EOF modes do not necessarily describe physical processes, a remarkable feature of our analysis is that, persisting through 4 modes of variability which altogether represent 82% of the total variance of the dataset, these two subcells appear to dominate the morphodynamics of the beach. These subcells were revealed because of two defining characteristics of our research: a high resolution spatial and temporal dataset, analyzed using a statistical method designed to identify underlying patterns.

We interpret trends in data variance to suggest that these east and west subcells usually operate independently, but sometimes share sand. Our interpretation is that individual modes of variability reveal the combined effect of longshore and cross-shore sediment transport trends. The EOF modes suggest that nearshore bathymetry plays a role in modulating wave energy resulting in distinct styles of sand transport. Again, DEM analysis and EOF modes 1, 2, and 4 identify a centrally-located subcell boundary. This subcell boundary corresponds to an outcrop of

fossil reef, which likely prevents the entire beach from operating as a single littoral cell and may also control sediment exchange with nearshore sand fields. The influence of this outcrop likely varies depending on the characteristics of waves and tides. Different directions of wave approach as well as wave energy, interacting with different states of the tide, will determine the water depth, flow direction, and energy of currents both on and around this outcrop, thus controlling sand transport.

5.2 Event-based Volume Displacement

Our data allow us to examine changes in sand volume associated with individual swell events that impacted the study area. There was an overall gain in sediment volume of 1384.8 ± 102.2 m^3 over the course of the monitoring period, but it was not monotonic; individual erosion and accretion events have the capacity to displace several hundred cubic meters of sediment.

A series of seven high energy wave events occurred between mid-May and late-June. Cumulatively, they correspond to a beach volume gain of ~370 ± 101.7 m^3. Individual swell events show relatively small gains in volume. For example, one swell event occurred between June 6-14 with a significant wave height (h_s) of 1.3 m and arrived from a direction of 212º (SW/SSW). It led to a gain of 53.2 ± 103.1 m^3 of sediment. This swell saw a mean and peak period of 8-9 seconds and ~20 seconds, respectively. A second swell, occurring between June 14-21 with a slightly smaller h_s of 1 m, but with a similar direction and period as the first event, led to a beach volume gain of 68.4 ± 103.5 m^3. The smaller of the swells appears to have displaced a larger amount of sand. We hypothesize that smaller waves may be able to travel across the nearshore reef platform without significant energy dissipation, driving larger displacements of sediment.

Hurricanes produced the largest of the swells during the monitoring period. These swell events did not interrupt previously existing accretion trends, nor produce decreases in beach area or volume. Hurricane swells are different from swells originating in the southern hemisphere in that they usually result in relatively brief, short period waves from several directions as the storm system passes. Depending on the distance to the hurricane, they are also capable of disrupting wind speed and direction. Hurricane Lane, for instance, impacted the study area at the end of August and generated the largest swell of the monitoring period. However, due to its approach

from the east, winds associated with the storm came from the same direction as the trade-winds, but were of greater speed, peaking at 4.8 m/s. Beach area and volume show an increase (surface area gained 226 ± 39.7 m^2, volume grew 270 ± 105.3 m^3) at the same time that swell from Hurricane Lane occurred in the study area. Owing to the weekly sample spacing of our database, it is not possible to discern if Hurricane Lane swell was responsible for this accretion trend or if its effect was to not interrupt an existing trend.

Besides swell, periods of wind variability correlate with short-term sediment displacement. Two episodes of wind variability, one in late-May and the other occurring throughout the month of September, correspond to relatively large erosion events. In late-May, 964.2 ± 97.5 m^3 of sediment were eroded, and in September 1233.0 ± 103.7 m^3 were lost. During both episodes, changes in winds drove changes in wave direction. Although h_s did not exceed 1 m, the eroded volumes exceeded sediment displacements related to southern hemisphere swells and local hurricanes. We interpret this as indicating that local, wind-generated marine forcing, or lack thereof, may either be a significant driver of sediment transport in the study area or allow for more effective transport of sediment via waves, tides, and associated currents.

5.3 Seasonal Variability

Net sediment volume within the study area shows variability that appear to be consistent with seasonal shifts in wave direction and found in previous studies. Our first survey (mid-April), captures the beach before it has been influenced by the season of high wave energy. As swells impact the study area, sediment volume increases until early November. The study area tends to accumulate sand as swell energy dominates the mechanisms of transport.

6. CONCLUSIONS

Results from weekly survey data between April and November of 2018 illustrate the efficacy of low-cost, consumer-grade sUAS and their use in coastal monitoring. We demonstrate that the collection of high spatial resolution datasets provide insight into beach morphodynamics, allowing the identification of unique modes of sediment exchange. This advance is especially useful given the site-specific conditions that develop on carbonate beaches due to the complex

bathymetry of fringing reefs. We have also shown that monitoring carbonate beaches, which are underrepresented in the global literature, can be performed in an affordable way and yield insights to their behavior that can inform management decisions. This is critical given their high economic value in the global tourism economy.

Surface variability and EOF analyses reveal subcell behavior of the study area in which the east and west halves of the beach appear to both function independently as well as share sand. Spatial patterns indicate that subcell behavior is influenced by marine forcing associated with wind-generated wave conditions and wave interaction with the nearshore reef. The centrally-located border between the two subcells, where a shallow reef outcrop abuts the subaerial beach, may be indicative of this interaction.

Overall, the net increase in surface area and volume of the beach over the course of the monitoring period is consistent with previous studies citing seasonal shifts in wave direction. We find that episodes of swell, annually confined to Northern Hemisphere summer, result in an overall increase in beach volume. This net increase was punctuated by losses and gains associated with swell events, storms, and periods of wind variability. Swell generated from both Southern Hemisphere storms, and regional cyclonic weather systems, correspond to gains in sediment volume. Local wind-generated marine forcing may be a significant driver of sediment transport in the study area.

These data will assist managers, engineers, and other stakeholders in developing strategies to sustain Royal Hawaiian Beach. Considering the economic, ecological, recreational, and cultural value of carbonate beaches, we see these techniques as globally applicable. Given the likely continuation and acceleration of global mean sea level rise, many levels of stakeholders are invested in sustaining these high-value beaches for as long as possible. For these reasons and more, affordable, high resolution systems, like consumer-grade sUAS used in this study, prove to be a valuable tool for the management of coastal areas.

References Cited

Anderson, T.R., Frazer, L.N., and C.H. Fletcher, 2010, Transient and persistent shoreline change from a storm, Geophysical Research Letters, L08401, doi:10.1029/2009GL042252

Aubrey, D. G. (1979). Seasonal patterns of onshore/offshore sediment movement. *Journal of Geophysical Research*, *84*(C10), 6347. https://doi.org/10.1029/JC084iC10p06347

Beretta, F., Shibata, H., Cordova, R., Peroni, R. de L., Azambuja, J., & Costa, J. F. C. L. (2018). Topographic modelling using UAVs compared with traditional survey methods in mining. *REM - International Engineering Journal*, *71*(3), 463–470. https://doi.org/10.1590/0370-44672017710074

Casella, E., Rovere, A., Pedroncini, A., Stark, C. P., Casella, M., Ferrari, M., & Firpo, M. (2016). Drones as tools for monitoring beach topography changes in the Ligurian Sea (NW Mediterranean). *Geo-Marine Letters*, *36*(2), 151–163. https://doi.org/10.1007/s00367-016-0435-9

Clark, J.R.K., 1977. The Beaches of O'ahu. University of Hawaii Press. Honolulu, HI. 193 pp.

Coyne, M. A., Fletcher, C. H., & Richmond, B. M. (1999). *Mapping Coastal Erosion Hazard Areas in Hawaii: Observations and Errors*. 171–184.

Dail, H. J., Merrifield, M. A., & Bevis, M. (2000). Steep beach morphology changes due to energetic wave forcing. *Marine Geology*, *162*(2–4), 443–458. https://doi.org/10.1016/S0025-3227(99)00072-9

Dean, R. G. (2003). *Beach nourishment: theory and practice* (Vol. 18). World Scientific Publishing Company.

Delacourt, C., Allemand, P., Jaud, M., Grandjean, P., Deschamps, A., Ammann, J., … Suanez, S. (2009). DRELIO: An unmanned helicopter for imaging coastal areas. *Journal of Coastal Research*, (56), 6.

Dolan, R., Hayden, B., & Heywood, J. (1978). A new photogrammetric method for determining shoreline erosion. *Coastal Engineering*, *2*, 21–39. https://doi.org/10.1016/0378-3839(78)90003-0

Environmental Assessment, Sea Engineering, 2010. Waikiki beach maintenance, Honolulu, Hawaii. Prepared by Sea Engineering, Inc. for Hawaii DLNR, Job No. 25172

Fletcher, C., Rooney, J., Barbee, M., Lim, S., & Richmond, B. (2003). Mapping Shoreline Change Using Digital Orthophotogrammetry on Maui, Hawaii. *Journal of Coastal Research,* 106-124.

Fletcher, C.H., Romine, B.M., Genz, A.S., Barbee, M.M., Dyer, M., Anderson, T.R., Lim, S.C., Vitousek, S., Bochicchio, C., and Richmond, B.M., 2012, National assessment of shoreline change: Historical shoreline change in the Hawaiian Islands: U.S. Geological Survey Open-File Report 2011–1051, 55 p.

Genz, A. S., Fletcher, C. H., Dunn, R. A., Frazer, L. N., & Rooney, J. J. (2007). The Predictive Accuracy of Shoreline Change Rate Methods and Alongshore Beach Variation on Maui, Hawaii. *Journal of Coastal Research*, *231*, 87–105. https://doi.org/10.2112/05-0521.1

Gerritsen, F., 1978. Beach and Surf Parameters in Hawaii. University of Hawaii, Sea Grant College Program.

Habel, S., Fletcher, C. H., Barbee, M., & Anderson, T. R. (2016). The influence of seasonal patterns on a beach nourishment project in a complex reef environment. *Coastal Engineering*, *116*, 67–76. https://doi.org/10.1016/j.coastaleng.2016.06.006

Hallermeier, R. J. (n.d.). USES FOR A CALCULATED LIMIT DEPTH TO BEACH EROSION. *COASTAL ENGINEERING*, 20.

Harley, M. D., Turner, I. L., Short, A. D., & Ranasinghe, R. (2011). Assessment and integration of conventional, RTK-GPS and image-derived beach survey methods for daily to decadal coastal monitoring. *Coastal Engineering*, *58*(2), 194–205. https://doi.org/10.1016/j.coastaleng.2010.09.006

Holman, R. A., & Stanley, J. (2007). The history and technical capabilities of Argus. *Coastal Engineering*, *54*(6–7), 477–491. https://doi.org/10.1016/j.coastaleng.2007.01.003

Homer, P.S., 1964. Characteristics of deep water waves in Oahu area for a typical year. Prepared for the Board of Harbor Commissioners, State of Hawaii. Contract No. 5772. Marine Advisors, La Jolla, California.

Lomax, A. S., Corso, W., & Etro, J. F. (2005). Employing Unmanned Aerial Vehicles (UAVs) as an Element of the Integrated Ocean Observing System. *Proceedings of OCEANS 2005 MTS/IEEE*, 1–7. https://doi.org/10.1109/OCEANS.2005.1639759

Losada, M. A., Medina, R., Vidal, C., & Roldan, A. (1991). Historical evolution and morphological analysis of" El Puntal" spit, Santander (Spain). *Journal of Coastal research*, 711-722.

Mancini, F., Dubbini, M., Gattelli, M., Stecchi, F., Fabbri, S., & Gabbianelli, G. (2013). Using Unmanned Aerial Vehicles (UAV) for High-Resolution Reconstruction of Topography: The Structure from Motion Approach on Coastal Environments. *Remote Sensing*, *5*(12), 6880–6898. https://doi.org/10.3390/rs5126880

Miller, T. L., & Fletcher, C. H. (2003). Waikiki: Historical Analysis of an Engineered Shoreline. *Journal of Coastal Research*, *19*(4), 1026–1043.

Moberly RM, Chamberlain T (1964). Hawaiian beach systems. Honolulu, Hawaii: University of Hawaii, Institute of Geophysics, Final Report HIG-64-2

Murakami, H., Wang, B., Li, T., & Kitoh, A. (2013). Projected increase in tropical cyclones near Hawaii. *Nature Climate Change*, *3*(8), 749–754. https://doi.org/10.1038/nclimate1890

NOAA National Centers for Environmental Information, State of the Climate: Hurricanes and Tropical Storms for Annual 2018, published online January 2019, retrieved on November 7, 2019 from https://www.ncdc.noaa.gov/sotc/tropical-cyclones/201813.

NOAA Tides and Currents, 2003. https://tidesandcurrents.noaa.gov/datums.html?datum=MSL&units=1&epoch=0&id=1612340&name=Honolulu&state=HI

Norcross, Z. M. N., Fletcher, C. H., Rooney, J. J. R., Eversole, D., & Miller, T. L. (n.d.). *HAWAIIAN BEACHES DOMINATED BY LONGSHORE TRANSPORT*. 15.

Pacific Islands Ocean Observing System (PacIOOS). (2016). Mean Higher High Water (MHHW) Sea Level: Honolulu, Hawaii. NOAA Coastal Storms Program. https://www.pacioos.hawaii.edu/metadata/hi_csp_hono_mhhw.html

Romine, B. M., & Fletcher, C. H. (2013). A Summary of Historical Shoreline Changes on Beaches of Kauai, Oahu, and Maui, Hawaii. *Journal of Coastal Research*, *288*, 605–614. https://doi.org/10.2112/JCOASTRES-D-11-00202.1

Rooney, J. J. B., & Fletcher, C. H. (1983). *A High Resolution, Digital, Aerial Photogrammetric Analysis of Historical Shoreline Change and Net Sediment Transport Along the Kihei Coast of Maui, Hawaii*. 18.

"Simulating WAves Nearshore (SWAN) Regional Wave Model: Oahu" (2010). Pacific Islands Ocean Observing System (PacIOOS). http://www.pacioos.hawaii.edu/metadata/swan_oahu.html

Stockdon, H. F., & Sallenger, A. H. (n.d.). *Estimation of Shoreline Position and Change using Airborne Topographic Lidar Data*. 12.

Tarui, N., Peng, M., Eversole, D. *Economic Impact Analysis of the Potential Erosion of Waikiki Beach*. April, 2018. University of Hawai'i Sea Grant College Program.

Turner, I. L., Harley, M. D., & Drummond, C. D. (2016). UAVs for coastal surveying. *Coastal Engineering*, *114*, 19–24. https://doi.org/10.1016/j.coastaleng.2016.03.011

USGS (2017a). Agisoft Photoscan Workflow. United States Geological Survey. https://uas.usgs.gov/nupo/pdf/USGSAgisoftPhotoScanWorkflow.pdf

USGS (2017b). Notes from Photoscan workshop, Denver, CO, 29 Jan. - 3 Feb. 2017, version 1.2.6. United States Geological Survey. UAS Federal Users Workshop 2017. https://my.usgs.gov/confluence/pages/viewpage.action?pageId=563130595

Vautherin, J., Rutishauser, S., Schneider-Zapp, K., Choi, H. F., Chovancova, V., Glass, A., … Sa, D. (2016). Photogrammetric accuracy and modeling of rolling shutter cameras. *ISPRS Journal of Photogrammetry and Remote Sensing*, *3*(3), 139–146.

Vitousek, S., & Fletcher, C. H. (2008). Maximum Annually Recurring Wave Heights in Hawai‘i. *Pacific Science*, *62*(4), 541-553.

Wang, N., & Gerritsen, F. (1995). Nearshore circulation and dredged material transport at Waikiki Beach. *Coastal Engineering*, *24*(3–4), 315–341. https://doi.org/10.1016/0378-3839(94)00032-S

Wave Forecast: PacIOOS. Pacific Islands Ocean Observing System (PacIOOS) Available at: http://www.pacioos.hawaii.edu/waves-category/model/. (Accessed: 3rd December 2018)

White, S. A., & Wang, Y. (2003). Utilizing DEMs derived from LIDAR data to analyze morphologic change in the North Carolina coastline. *Remote Sensing of Environment*, *85*(1), 39–47. https://doi.org/10.1016/S0034-4257(02)00185-2

Wiegel, R. L. (2008). *Waikiki Beach, Oahu, Hawaii: History of its transformation from a natural to an urban shore*. *76*(2), 28.

Winant, C. D., Inman, D. L., & Nordstrom, C. E. (1975). Description of seasonal beach changes using empirical eigenfunctions. *Journal of Geophysical Research*, *80*(15), 1979–1986. https://doi.org/10.1029/JC080i015p01979

Wind Forecast: PacIOOS. Pacific Islands Ocean Observing System (PacIOOS) Available at: http://www.pacioos.hawaii.edu/weather-category/model-wind/. (Accessed: 3rd December 2018)